PCCP

Accepted Manuscript

ROYAL SOCIETY OF CHEMISTRY

www.rsc.org/pccp

Journal Name

ARTICLE

Life of superoxide in aprotic Li-O_2 battery electrolytes: simulated solvent and counter-ion effects

J. Scheers,[a] D. Lidberg,[a] K. Sodeyama,[b] Z. Futera[b] and Y. Tateyama[b-e]

Received 00th January 20xx,
Accepted 00th January 20xx

DOI: 10.1039/x0xx00000x

www.rsc.org/

The Li-air battery ideally makes use of oxygen from the atmosphere and metallic lithium to reversibly drive the reaction 2Li + $O_2 \leftrightarrow Li_2O_2$. Conceptually, energy throughput is high and material use efficient, but practically many material challenges remain. It is of particular interest to control the electrolyte environment of superoxide (O_2^{*-}) to promote or hinder specific reaction mechanisms. By combining Density Functional Theory based Molecular Dynamics (DFT-MD) and DFT simulations we probe the bond length and electronic properties of O_2^{*-} in three aprotic solvents – in the presence of Li^+ or the much larger cation alternative tetrabutylammonium (TBA^+). Contact ion pairs, LiO_2^*, are favoured over solvent-separated ion pairs in all solvents, but particularly in low permittivity dimethoxyethane (DME), which makes O_2^{*-} more prone to further reduction. The Li^+-O_2^{*-} interactions are dampened in dimethyl sulfoxide (DMSO), relative DME and propylene carbonate (PC), which is reflected in smaller changes in the electronic properties of O_2^{*-} in DMSO. The additive TBA^+ offers an alternative, more weakly interacting partner to O_2^{*-}, that makes it easier to remove the unpaired electron and makes oxidation more feasible. In DMSO, TBA^+ has close to no effect on O_2^{*-}, which behaves as if no cation is present. This is contrasted by a much stronger influence of TBA^+ on O_2^{*-} in DME – comparable to that of Li^+ in DMSO. An important future goal is to compare and rank the effects of different additives beyond TBA^+. Here, the results of DFT calculations for small-sized cluster models are in qualitative agreement with those of the DFT-MD simulations, which suggests the cluster approach to be a cost-effective alternative to the DFT-MD simulations for a more extensive comparison of additive effects in future studies.

Introduction

The Li-air battery is an attractive electrochemical energy storage technology for the future; in the best of worlds the combination of a lithium metal anode and an oxygen-breathing cathode will enable a battery system with a capacity competitive with gasoline powered technologies[1]. Thus, a strong incentive exists to develop the Li-air battery into *"the"* technology of choice for energy demanding and cost-sensitive storage applications. However, despite progress in recent years, considerable challenges remain before a practical, reversible, Li-air battery can be developed[2]. These challenges must be solved in ways that conserve the theoretical advantages of the Li-air battery – not to forfeit its purpose.

Reversible Li–O_2 electrochemistry is mainly hindered by poor solvent stability in the presence of the reduction products of O_2 (*e.g.* O_2^{*-}, LiO_2^*, O_2^{2-}, and Li_2O_2); the instability of propylene carbonate (PC) being the most well-known example[3,4]. The reactivity and decomposition mechanisms of suggested solvents for Li-O_2 batteries have since been devoted much effort[5–16], but to date it has been difficult to find or predict new, stable, solvents for future use, and there are no guarantees that such unique and robust solvents exist. Therefore, alternative approaches may be needed to improve the electrolyte stability. Furthermore, electrolyte stability is not the only prerequisite; a practical, rechargeable Li-O_2 battery requires an electrolyte with facile ion transport and both a reversible and favourable path between O_2 and Li_2O_2. The formation of thin, nanometer thick, conformal layers of Li_2O_2, for example, is an unwanted outcome that block further reactions and severely limit the energy output of the battery[17].

The electrolyte composition has recently been demonstrated to play a crucial role to promote the growth of large micro-sized Li_2O_2 particles and much improved discharge capacities of Li-O_2 batteries[18]. Solvents with high donor and/or acceptor numbers seem to be key, already at additive concentrations, to dissolve and solvate LiO_2 in a solution mediated Li_2O_2 growth mechanism[18,19]. Ionic additives provide a similar function[20,21] and, overall, an additive approach is likely needed to meet the diverse functions requested in the Li-O_2 battery; additives that form complexes with Li^+, O_2^{*-} and O_2, promote Li_2O_2 dissociation, and serve additional functions[20–23].

Superoxide (O_2^{*-}) and LiO_2^* are two experimentally observed[24] radical intermediates suggested to influence both solvent decomposition and Li_2O_2 growth. It is of interest to investigate their properties in Li-O_2 electrolytes, as a function of solvent and additives, to understand the influence over electrolyte properties and in the long run battery performance (Fig. 1). We here make use of Density Functional Theory based Molecular Dynamics (DFT-MD) simulations and quantum chemistry calculations of model systems to probe changes in

O_2^{*-} properties as a function of shifting surroundings; dimethoxyethane (DME), dimethyl sulfoxide (DMSO), or PC – contact or no contact with Li^+. The selection of solvents is motivated by their wide use in Li-air battery research and contrasting properties; DME being a medium donor number and low permittivity solvent, DMSO having a high donor number and medium permittivity, and PC of high permittivity and low donicity (Table 1). The computational approach makes it possible to study these electrolytes without the bias of solvent decomposition, impurities etc.

The results suggest that the solubility of LiO_2^* is governed mainly by the solvent permittivity, while weaker Li^+-O_2^{*-} interactions and a lower reduction potential of LiO_2^* in DMSO are explained in terms of a higher solvent donor number. By replacing Li^+ with tetrabutylammonium (TBA^+), we take a first step towards screening for additive effects. TBA^+ is shown to interact only very weakly with O_2^{*-} in DMSO and, thus, have little influence over its properties in the electrolyte. The effects are, however, much stronger in DME.

Computational details

Car-Parrinello Molecular Dynamics (CPMD)[25,26] DFT-MD was used to simulate LiO_2^* solvation in DME, DMSO, and PC (Table 1). Three simulation boxes with 30 DME, 36 DMSO, and 36 PC molecules were setup and pre-equilibrated using classical MD (Amber). The CPMD simulations were then initiated by introducing one LiO_2^* *contact ion pair* (CIP), in place of one solvent molecule, in each of the cubic super cells; 29 DME + 1 LiO_2^* (a=17.37 Å, □=0.84 g/cm^3), 35 DMSO + 1 LiO_2^* (a=16.23 Å, □=1.08 g/cm^3), and 35 PC + 1 LiO_2^* (a=17.20 Å, □=1.18 g/cm^3). Three additional electrolytes were setup by separating Li^+ from O_2^{*-} to model the corresponding *solvent-separated ion pairs* (SSIP). It was confirmed from the final snapshots of all SSIP simulations that no CIP formation had occurred (suppl. Figure S9). The DMSO simulations were further modified by replacing TBA^+ for Li^+ and four DMSO molecules to give two additional electrolytes (CIP and SSIP) based on 1 TBA^+, 1 O_2^{*-}, and 31 DMSO molecules (a=16.23, □= g/cm^3). All simulations were performed with periodic boundary conditions (PBC) and correspond to salt concentrations of 0.3-0.4 mol/dm^3. Total energies were calculated at the Γ-point with the PBE generalized gradient corrected exchange-correlation functional[27,28].

Table 1 Solvent permittivity (ε), donor (DN), acceptor number (AN), and density as reported in literature[29].

Solvent	ε	DN	□□	ρ/g cm^{-3}
DME	7.2	20.0	10.2	0.87
DMSO	48.0	29.8	19.3	1.10
PC	64.9	15.1	18.3	1.20

The fictious electron mass was 500 au, the time step 4 au (0.1 fs), and the orbital convergence 10^{-5} au. Stefan Goedecker's norm-conserving pseudopotentials[30–32] were used (for H, Li, C, N, O, and S). A Nosé thermostat[33,34] was implemented to keep the temperature at 353 K. The spin multiplicity was two, due to the unpaired electron in O_2^{*-}. Equilibration was performed for 10 ps, followed by an additional 10 ps production runs. Every picosecond, or less, the electronic wave function was quenched to the Born-Oppenheimer surface to maintain adiabaticity. The product runs were subject to analysis of bond trajectories and radial distribution functions. Ten snapshots, at 1 ps intervals, were used to calculate the wavefunction and projected density of states of the electrolytes. The latter were used to identify the frontier orbital energies. An additional 10 ps of simulations for PC, and 20 ps for DMSO, were made to assess the convergence of the simulations over longer time-scales.

Small clusters of explicitly solvated O_2^{*-} and LiO_2^* were extracted from CPMD-snapshots and geometry optimized in Gaussian 09 (RevB.01)[35]. The clusters included six explicit solvent molecules. The B3LYP exchange-correlation functional[36] was used together with the 6-31G(d) Pople basis set, in vacuum or using a polarizable continuum model (PCM)[37]. The default PCM settings were used for diethylether (DEE) and DMSO, while DME (□=7.2) and PC (□=64.9) were modelled using these non-default dielectric constants together with the DMSO PCM. The low permittivity DEE PCM was included as a second common reference for all complexes, in addition to the vacuum reference. The purpose of using a common continuum reference for models with different explicit solvents was to highlight possible differences related to the explicit interactions and the interactions with the continuum medium. Adding or subtracting an electron and re-optimizing the structures, the reduction and oxidation properties of the clusters were addressed; adiabatic electron affinities (EA) were calculated as the energy difference of the reduced and original clusters, and adiabatic ionization potentials (IP) as the difference between oxidized and original clusters. Singlet (M=1) reduction products and triplet multiplicity (M=3) oxidation products were favoured in all electrolytes.

Clusters with $[TBA]^+[O_2]^{*-}$ or $[TBA]^+[LiO_2]^{*-}$ were setup by replacing part of the explicit solvent molecules in the corresponding geometry optimized O_2^{*-} and LiO_2^* cluster models. The final clusters included two or three explicit solvent molecules.

Results and discussion

LiO_2^* contact ion pairs (CIP) are favoured in DME, DMSO, and PC

O_2^{*-} and Li^+ can be in direct contact in the electrolytes to form contact ion pairs, CIP [LiO_2^*], or be separated by one or several layers of solvents in solvent-separated ion pairs and PC – altogether six electrolytes – show that the energies of the two states largely overlap, but on average CIP formation is preferred in all solvents (Fig. 3). It is difficult to estimate absolute energy differences, since energy convergence is slow for several electrolytes (Suppl. Fig. S1), but the relative results

are consistent and suggest a correlation with the solvent permittivity (Table 1):, SSIP [Li^+ + O_2^{*-}] (Fig. 2). DFT-MD simulations of the SSIP and CIP states in DME, DMSO,

$$\langle \Delta E_{CIP\text{-}SSIP} \rangle: \quad DME >> DMSO > PC$$

Additional information is provided by cluster-type quantum chemistry calculations of the LiO_2^* formation energy, ΔE_{CIP}, in explicit and implicit solvents (Fig. 4). In vacuum, or in a weak and common solvent continuum (DEE), the reaction energy follows the order DMSO > PC > DME, *i.e.* the stabilization of LiO_2^* is strongest in DMSO and weakest in DME. However, when increasing the strength of the continuum solvent and taking into account the appropriate permittivity of each electrolyte, the overall trend is similar to that of the DFT-MD simulations: DME > DMSO > PC. Thus, the cluster results highlight the relative impact of the explicit and continuum solvation.

A CIP preference is not surprising, since the presence of Li^+ is known to strongly influence the O_2/O_2^{*-} electrochemistry in each solvent[38], but the relative stability of CIP between solvents is not as intuitive. A high Gutmann donor number (DN) favours the solvation of Li^+, a high acceptor number (AN) the solvation of O_2^{*-}, which promotes the dissociation of the CIP into SSIP. A high permittivity solvent has the same qualitative effect of promoting CIP dissociation. The DN of solvents have been used to explain experimental differences in LiO_2 solubility[18], but the DFT-MD and cluster results here suggest the permittivity of the solvent to be a stronger determinant for the ionic association in the electrolyte than the DN. Despite PC being the solvent with the lowest DN it is suggested to be more efficient than DME or DMSO in solubilizing LiO_2^*, which can only be explained by its higher permittivity.

The O_2^{*-} bond length is longer in LiO_2^* CIP

The DFT-MD simulations estimate the O_2^{*-} bond length, rOO, in the CIP to be *ca*. 0.01Å longer than that of the SSIP. Although the difference is small, the two different "states" of O_2^{*-} are clearly distinguished in the bond distance trajectories (Fig. 5). Contrary to the CIP and SSIP differences, the average rOO is only weakly affected (10^{-3}Å) by the specific electrolyte solvent.

The Li-O_2 bond distance between Li^+ and the two O_2^{*-} oxygen atoms, rOLi, is on average *ca.* 0.1Å longer in the DMSO CIP electrolyte (2.07Å) than in DME and PC (1.93Å), which informs us of a Li^+ less tightly bound to O_2^{*-} in DMSO. Consequently, Li^+ is freer to move relative the individual oxygen atoms of O_2^{*-} – as observed in the bond length trajectories (Fig. 5); in particular, at 8 ps into the DMSO CIP trajectory, the Li^+ moves far from the centre of O_2^{*-} and rOO is contracted accordingly. The weaker interaction between O_2^{*-} and Li^+ in DMSO is, as suggested elsewhere [38], arguably a result of the higher DN of DMSO (Table 1), which provides a more efficient screening of the positive charge of Li^+. The statistical increase and wider distribution of rOO bond lengths, and the weaker interaction between Li^+ and O_2^{*-}, in the DMSO CIP electrolyte is summarized in the radial distribution function of O_2^{*-} (Suppl. Fig. S2).

The cluster approach supports an increase of the rOO bond lengths in DME and PC clusters when Li^+ is introduced to form a CIP with O_2^{*-}, although the absolute bond lengths are different and the overall structural differences are smaller (Suppl. Table S1). Part of the changes in absolute bond lengths can be attributed to the use of different functionals (Suppl. Table S2). No difference in rOO is found between the clusters of O_2^{*-} or LiO_2^* explicitly solvated in DMSO. However, this is also in accordance with the DFT-MD results, since the CIP cluster optimized in DMSO (Suppl. Fig. S3) is representative of the situation where Li^+ is coordinated only to one of the O_2^{*-} oxygen atoms – circumstances under which the DFT-MD rOO bond trajectory suggests a shorter rOO bond length (see DMSO trajectory at 9ps, Fig. 5).

The coordination of Li^+ is higher in DME and DMSO LiO_2^* CIP

The cumulative radial distribution functions, or coordination numbers (CN), from the DFT-MD simulations reveal an approximate 4-fold coordination of Li^+ by oxygen atoms in all SSIP electrolytes (Fig. 6). CIP formation increase the CN relative to the SSIP electrolytes for DME (3.8 → 4.2) and DMSO (3.8 → 4.3), but stays approximately the same for PC (3.9 → 4.0). In the CIP electrolytes the Li^+, per definition, host the two oxygen atoms of O_2^{*-}. Thus, in PC, O_2^{*-} almost exclusively replaces two solvent molecules when in the coordination sphere of Li^+, since the CN stays approximately the same. The higher CN of the DME and DMSO CIP electrolytes is interpreted as an increased probability for O_2^{*-} to replace a single solvent molecule, *i.e.* to replace one coordinating atom from the solvent with two from O_2^{*-}. The trend agrees with that of the DN where a higher donor number result in a more effective screening of Li^+. On top of this, other solvent properties, such as the size, conformational flexibility, and the number of possible coordination points per solvent, are likely to play an additional role for the coordination and solvation of LiO_2^*.

The structural differences in the surrounding of O_2^{*-} are smaller in the absence of Li^+ (SSIP electrolytes). The first solvation shell of O_2^{*-}, within a radius of *ca.* 2.8Å of any of the oxygen atoms, consists exclusively of hydrogen atoms from the solvent alkyl groups (Suppl. Fig. S4). As a result, controlling Li^+-O_2^{*-} interactions provide the best opportunity to influence the electrolyte properties, since at zero interaction the state of O_2^{*-} in any of the explored electrolytes will be very much the same.

Frontier orbital energies are lower in LiO_2^* CIP

The electronic energy levels of 10 snapshots from each DFT-MD simulation were analysed to determine the highest occupied and lowest unoccupied orbital (HOMO and LUMO) energies for each electrolyte. The HOMO levels, which are here singly occupied molecular orbitals (SOMO) due to the

unpaired electron, were in all cases located on O_2^{*-}. Therefore, the SOMO energy level provides a measure of the effects of the different environments on O_2^{*-}. The analysis reveals a stabilization of the average frontier orbital energies and increased SOMO-LUMO energy gaps in the CIP, relative to the SSIP electrolytes (Table 2).

The SOMO levels fluctuate over approximately one eV between snapshots, with a standard deviation of 0.2-0.3 eV (Suppl. Fig. S5). The average SSIP SOMOs are within 0.4 eV and follow the order; DME < DMSO < PC. The same order exists among the LUMO, but with a 0.9 eV separation of the lowest and highest energies. The SOMO-LUMO gap of DMSO and PC are of the same magnitude (*ca.* 0.6 eV) and larger than that of DME (0.2 eV).

The SOMO and LUMO energies of the CIP electrolytes are lower than for the SSIP; the LiO_2^* CIP stabilizes O_2^{*-} towards oxidation by the lower SOMO energy, but at the same time make reduction more likely by the lower LUMO levels (Table 2). DME is the solvent with the most pronounced stabilization of the frontier orbitals, while DMSO is the least affected. The magnitude of SOMO stabilization upon CIP formation is of the order of 2 eV for DME, 1.5 eV for PC, and 1 eV for DMSO (Table 2). The LUMO stabilization is smaller and somewhat stronger for DME and PC (*ca* 1.2 eV) than for DMSO (0.8 eV). The latter result is in qualitative agreement with the trend in DN (Table 1), but the stabilization of the occupied SOMO orbitals – the relative results for DME and PC – are not satisfactorily explained in terms of only the DN, which highlights the influence of other solvent parameters – the solvent permittivity being closest at hand.

The adiabatic ionization potentials (IP) and electron affinities (EA) of small clusters change according to the DFT-MD SOMO and LUMO

The small clusters with O_2^{*-} explicitly solvated by a few solvent molecules correspond to the SSIP electrolytes in the DFT-MD simulations. The EA and IP of O_2^{*-} in these clusters are sensitive to the use of an additional continuum solvent, as exemplified for DMSO (Fig. 7); in vacuum, all EA and IP are negative (reactions are endothermic) and of comparable energies, but already in a low permittivity solvent (DEE) the EV and IP become clearly separated.

With increasing permittivity (DME, DMSO, PC) the separation is 3-4 eV – all EA are negative (exothermic) and all IP endothermic. Thus, the explicit + implicit solvation cluster models suggest reduction to be favoured over oxidation, due to the stronger stabilization of the peroxide anion (O_2^{2-}) compared to molecular oxygen. The consistently higher EA of DME reflects not only a weaker permittivity, but also possibly a weaker ability of the less polar DME to stabilize the charge density of O_2^{2-}.

Table 2 Average SOMO and LUMO energies of CIP (LiO_2) and SSIP ($Li+O_2$) electrolytes. DFT-MD, 10 snapshots, T=353K.

Electrolyte	$\bar{\alpha}$ SOMO	$\bar{\alpha}$ LUMO	$\Delta\bar{\alpha}$ SOMO	$\Delta\bar{\alpha}$ LUMO
DME_{Li+O2}	2.48 ±0.23	2.68 ±0.26	–	–
$DMSO_{Li+O2}$	2.69 ±0.23	3.26 ±0.21	–	–
PC_{Li+O2}	2.89 ±0.24	3.45 ±0.27	–	–
DME_{LiO2}	0.52 ±0.31	1.45 ±0.24	-1.96	-1.23
$DMSO_{LiO2}$	1.71 ±0.31	2.47 ±0.27	-0.98	-0.79
PC_{LiO2}	1.34 ±0.34	2.26 ±0.33	-1.55	-1.19

The CIP cluster models, with LiO_2^* as the solvated species, are little affected by the continuum model (Suppl. Fig. S6). All EA are slightly more exothermic, and IP endothermic, compared to the SSIP cluster models (no Li^+), *i.e.* the CIP are more prone to reduction, but require a stronger oxidizing environment to be striped of an electron. This is anticipated based on the comparison of neutral with negatively charged clusters. The higher IP and lower EA of LiO_2^* relative O_2^{*-} are in qualitative agreement with the lower SOMO and LUMO energies of the CIP vs. SSIP electrolytes.

Quantitatively, the lower EA of the CIP over SSIP (ΔEA DME = -1.29 eV, DMSO = -0.59 and PC= -0.99 eV) are comparable to the DFT-MD ΔLUMO results (Fig. 8). The magnitudes of the positive ΔIP (DME=1.15 eV, DMSO/PC=*ca* 0.65 eV) are smaller compared to the negative ΔSOMO predicted by the DFT-MD models. The negative ΔSOMO correspond to positive IP, thus, plotting ΔSOMO as positive values eases a graphical comparison (Fig. 8).

The properties of O_2^{*-} are weakly influenced by $[TBA]^+[O2]^{*-}$ CIP

There are clear experimental differences in the redox behaviour of O_2/O_2^{*-} in electrolytes with or without Li^+ ions[23,24,38]. The use of the soft acid TBA^+ in place of Li^+, a hard acid, is said to stabilize the soft base O_2^{*-}, but what is meant by the term "stabilization" – can we in our simulations see signs of this stabilization in terms of changes in the properties of O_2^{*-} due to coordination with TBA^+?

DFT-MD simulations of two DMSO electrolytes with TBA^+ and O_2^{*-} (CIP and SSIP) suggest a small energy difference between the CIP and SSIP (Suppl. Fig. S7). The stabilization upon CIP formation is smaller compared to the electrolytes with Li^+. No difference in rOO between the SSIP and CIP of $TBAO_2$ is apparent and the SOMO and LUMO levels are similar (Table 3). The DFT-MD results suggest that the increased stability of O_2^{*-} in TBA^+ DMSO electrolytes is a result of the absence of, or at most only very weak, ion-ion interactions.

The formation energy of $[TBA]^+[O_2]^{*-}$ CIP in cluster models with two (DME) or three explicit solvent molecules (DMSO and PC) is negative and comparable in all solvents (ca -30 kcal mol^{-1}, Suppl. Fig. S8). Compared to the LiO_2^* formation energies (ca -70 to -90 kcal mol^{-1}) the energies are much smaller in case of TBA^+.

Table 3 Average rOO and SOMO/LUMO energies from TBA^+ CIP ($TBAO_2$) and SSIP ($TBA+O_2$) electrolytes. DFT-MD, 10 snapshots, T=353K.

Electrolyte	rOO /Å	$\bar{\alpha}$ SOMO /eV	$\bar{\alpha}$ LUMO /eV
$DMSO_{TBA+O2}$	1.370	2.56 ±0.34	3.09 ±0.31
$DMSO_{TBAO2}$	1.371	2.48 ±0.13	3.09 ±0.14

The same qualitative result holds when comparing the $[TBA]^+[O2]^{*-}$ and LiO_2^* CIP formation energies only in continuum solvents (not shown). The weak interactions of TBA^+ and O_2^{*-} is reflected also in the IP and EA of the corresponding cluster models (Fig. 8); the changes (ΔIP, ΔEA) relative the O_2^{*-} SSIP cluster models are small and almost zero in the case of ΔEA in DMSO – in accordance with the DFT-MD results (ΔLUMO=0).

Experimentally, Yu *et al.* have shown that a combination of in-situ spectroscopic and electrochemical techniques can be used to resolve the oxidation and reduction potentials of O_2^{*-} and LiO_2^* in DMSO[24]. LiO_2^* oxidation reaches a maximum at 3.7 V vs. Li/Li^+ (Au electrode; scan rate 10 mV/s), while oxidation of O_2^{*-} occur at 2.8 V vs. Li/Li^+ in a corresponding Li^+-free electrolyte (0.1M $TBAClO_4$ in DMSO). The experimental potential difference of 0.9V is in the region of the ΔIP (0.67 eV) and $|\Delta$SOMO| (0.79 eV) reported herein.

The kinetic influence over the experimental results makes reliable quantitative comparisons difficult, but the calculated results may still be of qualitative use. In the work of Johnson *et al.*, for example, only a *ca.* 0.05 V shift of the first anodic peak between 0.1M $LiClO_4$ and 0.1M $TBAClO_4$ DMSO electrolytes were reported[18] – when using a restricted potential window that avoided the second reduction step (to Li_2O_2) before the scan towards positive potentials. One interpretation is that LiO_2^* CIP in the corresponding electrolyte is not oxidized under the given experimental conditions, but only effect the reduction potential of O_2^{*-} via secondary changes in electrolyte properties, *e.g.* density, viscosity, or permittivity.

Conclusions

We have used computational simulations of simple models systems to show that O_2^{*-} is an internal probe of the molecular level environment in aprotic Li-O_2 battery electrolytes. When not directly coordinated to a cation, the bond length and electronic properties of O_2^{*-} is insensitive to the surrounding solvent (DME, DMSO, or PC) – assuming no decomposition reactions. When introducing Li^+, however, the formation of contact ion pairs (LiO_2^* CIP) are energetically favoured in all solvents, where LiO_2^* act to differentiate the electrolytes depending on solvent. LiO_2^* CIP are favoured in low permittivity media, why the strength of LiO_2^* formation follows the order: DME > DMSO > PC. As suggested elsewhere[38], the ion-ion interaction is dampened by the high donor number of DMSO – making Li^+ freer to move relative O_2^{*-} compared to in DME and PC electrolytes – here manifested in a weaker influence of Li^+ on the redox properties of O_2^{*-} in DMSO compared to in DME and PC.

With TBA^+ in place of Li^+, CIP formation is still favourable in all solvents, but in DMSO the O_2^{*-} experiences a situation much like that when no cation is present. Thus, the "stabilization" of O_2^{*-} in DMSO electrolytes with a TBA-salt resembles the situation of having no cation present. In DME, the presence of TBA^+ has considerable influence on the electronic properties of O_2^{*-} – comparable to the effects of Li^+ in DMSO. Since DME has a higher donor number than PC, in which the effects of TBA^+ are much weaker, the properties of O_2^{*-} are not simply governed by the solvent donor number. Solvent permittivity, but likely also other solvent differences, such as coordination number and mono- vs. multi-dentate coordination, play an important role in defining the O_2^{*-} environment.

The good correspondence of the results from, the comparatively simple and cost-effective, cluster-type quantum chemistry calculations with the much more computationally intensive DFT-MD simulations, suggest that the former can be used in future studies to screen for additive effects beyond TBA^+. More rigorous generation and optimization of clusters, as well as testing of different functional basis sets is out of the scope of this study, but will be valuable in future work. As of now, few rigorous computational studies have been performed of O_2^{*-} in aprotic electrolytes[39].

Finally, molecular oxygen is a physical contradiction in aprotic Li-O_2 battery electrolytes: it should be there as a cheap and abundant resource to reduce/oxidize to drive the reactions of the electrochemical cell – it should also not be there, since it generates species that drive parasitic decomposition reactions in most known solvents. The future of Li-O_2 batteries will depend on finding a clever resolution to this contradiction – resolving the conflict in time and/or space. Arguably, computational simulations will be of great use to find a solution. Despite difficulties making quantitative comparison with experimental data, because of the many parameters influencing experimental results, simple model systems will serve as a good test-bed for understanding fundamental differences in solubility, stability, which species to avoid or promote *etc*, in the quest for a practical Li-O_2 battery cell.

Acknowledgements

J.S. is grateful to the Japan Society for Promotion of Science (JSPS) for a short-term postdoctoral scholarship (FY2012 PE12543), the Swedish Energy Agency for the research grant "Development of future battery systems by atomistic modelling" (Pr37670-1), the Swedish National Allocation Committee (SNAC), Chalmers Centre for Computational Science and Engineering (C^3SE), and the National Supercomputer Centre (NSC) for computational resources.

References

1 Y. Shao, F. Ding, J. Xiao, J. Zhang, W. Xu, S. Park, J.-G. Zhang, Y. Wang and J. Liu, *Adv. Func. Mater.*, 2013, **23**, 987.
2 L. Grande, E. Paillard, J. Hassoun, J.-B. Park, Y.-J. Lee, Y.-K. Sun, S. Passerini and B. Scrosati, *Adv. Mater.*, 2014, **27**, 784.
3 F. Mizuno, S. Nakanishi, Y. Kotani, S. Yokoishi and H. Iba, *Electrochemistry*, 2010, **78**, 403.
4 S. A. Freunberger, Y. Chen, Z. Peng, J. M. Griffin, L. J. Hardwick, F. Bardé, P. Novák and P. G. Bruce, *J. Am. Chem. Soc.*, 2011, **133**, 8040.
5 V. S. Bryantsev, V. Giordani, W. Walker, M. Blanco, S. Zecevic, K. Sasaki, J. Uddin, D. Addison and G. V Chase, *J. Phys. Chem. A*, 2011, **115**, 12399.
6 R. Black, S. H. Oh, J. Lee, T. Yim, B. Adams and L. F. Nazar, *J. Am. Chem. Soc.*, 2012, **134**, 2902.
7 V. S. Bryantsev, J. Uddin, V. Giordani, W. Walker, D. Addison and G. V. Chase, *J. Electrochem. Soc.*, 2012, **160**, A160–A171.
8 V. S. Bryantsev and F. Faglioni, *J. Phys. Chem. A*, 2012, **116**, 7128–7138.
9 S. Das, J. Højberg, K. B. Knudsen, R. Younesi, P. Johansson, P. Norby and T. Vegge, *J. Phys. Chem. C*, 2015, **119**, 18084.
10 D. G. Kwabi, T. P. Batcho, C. V. Amanchukwu, N. Ortiz-Vitoriano, P. Hammond, C. V. Thompson and Y. Shao-Horn, *J. Phys. Chem. Lett.*, 2014, **5**, 2850.
11 T. Laino and A. Curioni, *Chem. - A Eur. J.*, 2012, **18**, 3510.
12 T. Laino and A. Curioni, *New J. Phys.*, 2013, **15**, 095009.
13 M. A. Schroeder, N. Kumar, A. J. Pearse, C. Liu, S. B. Lee, G. W. Rubloff, K. Leung and M. Noked, *ACS Appl. Mater. Interfaces*, 2015, **7**, 11402.
14 K. U. Schwenke, S. Meini, X. Wu, H. A. Gasteiger and M. Piana, *Phys. Chem. Chem. Phys.*, 2013, **15**, 11830.
15 R. Younesi, P. Norby and T. Vegge, *ECS Electrochem. Lett.*, 2014, **3**, A15.
16 Y. Okamoto and Y. Kubo, *J. Phys. Chem. C*, 2013, **117**, 15940–15946.
17 V. Viswanathan, K. S. Thygesen, J. S. Hummelshøj, J. K. Nørskov, G. Girishkumar, B. D. McCloskey and A. C. Luntz, *J. Chem. Phys.*, 2011, **135**, 214704.
18 L. Johnson, C. Li, Z. Liu, Y. Chen, S. A. Freunberger, P. C. Ashok, B. B. Praveen, K. Dholakia, J.-M. Tarascon and P. G. Bruce, *Nat. Chem.*, 2014, **6**, 1091.
19 N. B. Aetukuri, B. D. McCloskey, J. M. García, L. E. Krupp, V. Viswanathan and A. C. Luntz, *Nat. Chem.*, 2015, **7**, 50.
20 C. M. Burke, V. Pande, A. Khetan, V. Viswanathan and B. D. McCloskey, *Proc. Natl. Acad. Sci.*, 2015, **112**, 9293.
21 D. Sharon, D. Hirsberg, M. Afri, F. Chesneau, R. Lavi, A. A. Frimer, Y.-K. Sun and D. Aurbach, *ACS Appl. Mater. Interfaces*, 2015, **7**, 16590.
22 M. Balaish, A. Kraytsberg and Y. Ein-Eli, *Phys. Chem. Chem. Phys.*, 2014, **16**, 2801.
23 C. Li, O. Fontaine, S. A. Freunberger, L. Johnson, S. Grugeon, P. G. Bruce and M. Armand, *J. Phys. Chem. C*, 2014, **118**, 3393.
24 Y. Qiao and S. Ye, *J. Phys. Chem. C*, 2015, **119**, 12236.
25 R. Car and M. Parrinello, *Phys. Rev. Lett.*, 1985, **55**, 2471.
26 CPMD, *Car-Parrinello Molecular Dynamics, www.cpmd.org*
27 J. P. Perdew, K. Burke and M. Ernzerhof, *Phys. Rev. Lett.*, 1996, **77**, 3865–3868.
28 J. P. Perdew, K. Burke and M. Ernzerhof, 1997, **8730**, 46920.
29 Y. Marcus, *Chem. Soc. Rev*, 1993, **22**, 409.
30 S. Goedecker, M. Teter and J. Hutter, *Phys. Rev. B*, 1996, **54**, 1703.
31 C. Hartwigsen, S. Goedecker and J. Hutter, *Phys. Rev. B*, 1998, **58**, 3641.
32 M. Krack, *Theor. Chem. Acc.*, 2005, **114**, 145.
33 S. Nosé, *J. Chem. Phys.*, 1984, **81**, 511.
34 W. G. Hoover, 1985, **31**, 1695.
35 Gaussian 09, Revision B.01, M. J. Frisch, G. W. Trucks, H. B. Schlegel, G. E. Scuseria, M. A. Robb, J. R. Cheeseman, G. Scalmani, V. Barone, B. Mennucci, G. A. Petersson, H. Nakatsuji, M. Caricato, X. Li, H. P. Hratchian, A. F. Izmaylov, J. Bloino, G. Zheng, J. L. Sonnenberg, M. Hada, M. Ehara, K. Toyota, R. Fukuda, J. Hasegawa, M. Ishida, T. Nakajima, Y. Honda, O. Kitao, H. Nakai, T. Vreven, J. A. Montgomery, Jr., J. E. Peralta, F. Ogliaro, M. Bearpark, J. J. Heyd, E. Brothers, K. N. Kudin, V. N. Staroverov, R. Kobayashi, J. Normand, K. Raghavachari, A. Rendell, J. C. Burant, S. S. Iyengar, J. Tomasi, M. Cossi, N. Rega, J. M. Millam, M. Klene, J. E. Knox, J. B. Cross, V. Bakken, C. Adamo, J. Jaramillo, R. Gomperts, R. E. Stratmann, O. Yazyev, A. J. Austin, R. Cammi, C. Pomelli, J. W. Ochterski, R. L. Martin, K. Morokuma, V. G. Zakrzewski, G. A. Voth, P. Salvador, J. J. Dannenberg, S. Dapprich, A. D. Daniels, Ö. Farkas, J. B. Foresman, J. V. Ortiz, J. Cioslowski, and D. J. Fox, Gaussian, Inc., Wallingford CT, 2009.
36 A. D. Becke, *J. Chem. Phys.*, 1993, **98**, 5648.
37 S. Miertus, E. Scrocco and J. Tomasi, *Chem. Phys.*, 1981, **55**, 117.
38 C. O. Laoire, S. Mukerjee, K. M. Abraham, E. J. Plichta and M. A. Hendrickson, *J. Phys. Chem. C*, 2010, **114**, 9178.
39 V. S. Bryantsev, *Theor. Chem. Acc.*, 2012, **131**, 1250.

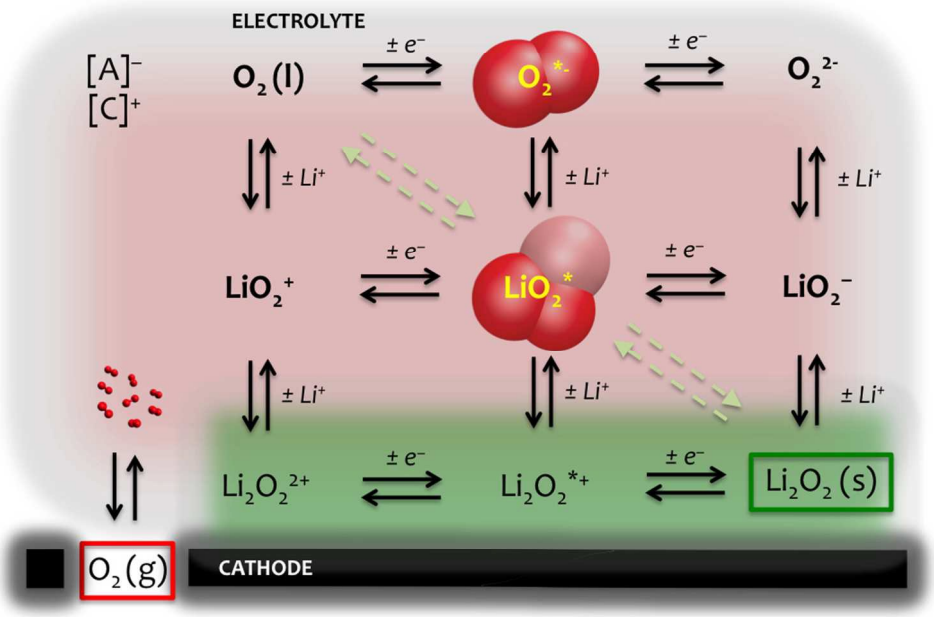

Figure 1 Possible reaction pathways between O_2 and Li_2O_2 in aprotic Li-O_2 battery electrolytes.
188x130mm (150 x 150 DPI)

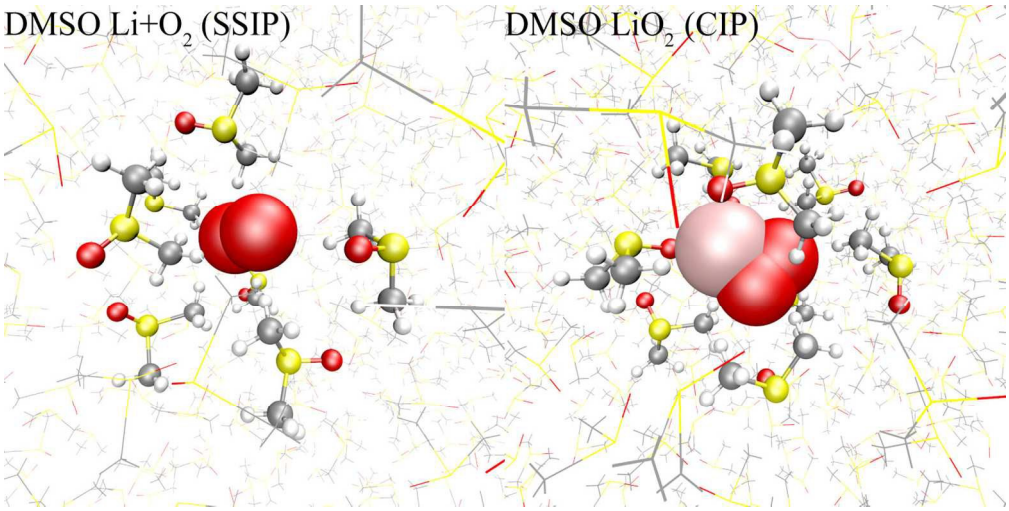

Figure 2 Representative snapshots from a solvent-separated ion pair (SSIP, left) and contact ion pair (CIP, right) in DMSO electrolytes. Li^+ (pink) and O_2*– (red) species are highlighted by space-fill models, the nearest solvents as ball-and-stick models, and the remaining solvents by wire representations.
135x67mm (300 x 300 DPI)

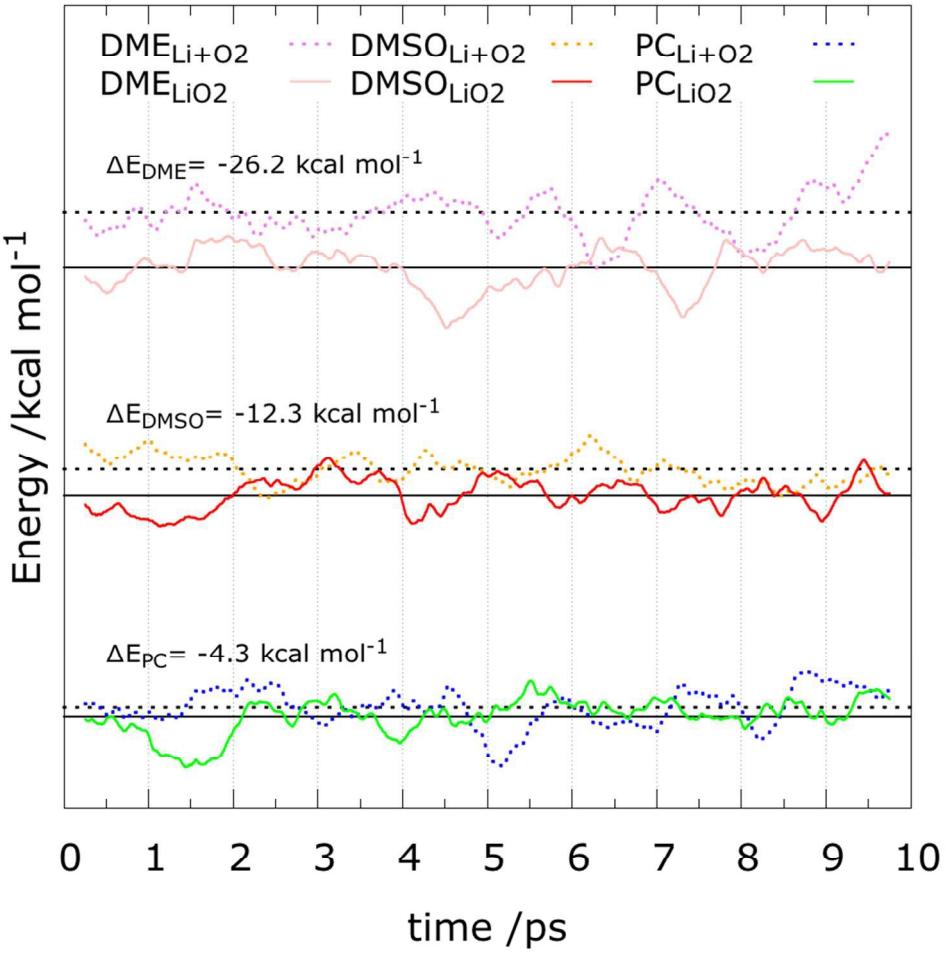

Figure 3 Running averages (0.5 ps) and total energy averages (10 ps) of LiO_2^* (solid) or $Li^+ + O_2^{*-}$ (dotted) trajectories from DFT-MD simulations of DME (top), DMSO (center), and PC (bottom). CIP formation is exothermic in all electrolytes. Absolute energies have been shifted to ease comparison. T=353K, t=10 ps. 369x369mm (72 x 72 DPI)

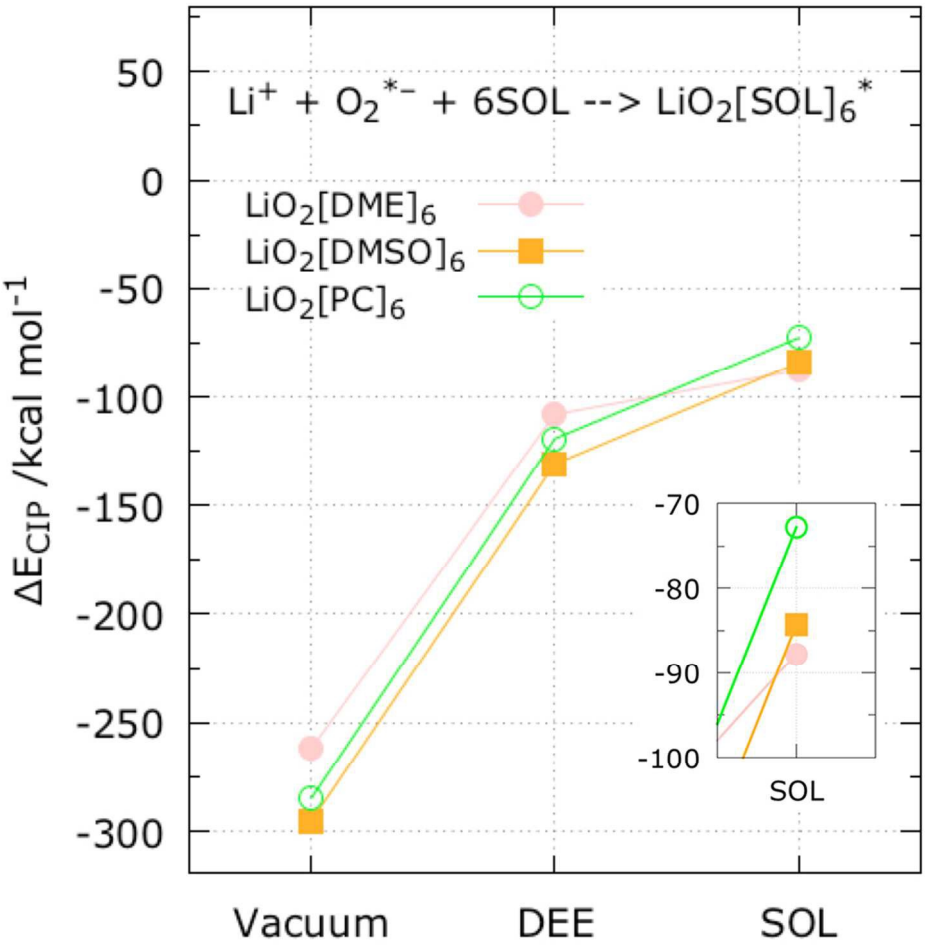

Figure 4 Energy of LiO_2^* CIP formation (ΔE_{CIP}) in a cluster with six explicit solvent molecules of DME, DMSO, or PC and a PCM continuum solvent (Vacuum, DEE, or SOL=DME, DMSO, PC). B3LYP/6-31G(d).
183x179mm (144 x 144 DPI)

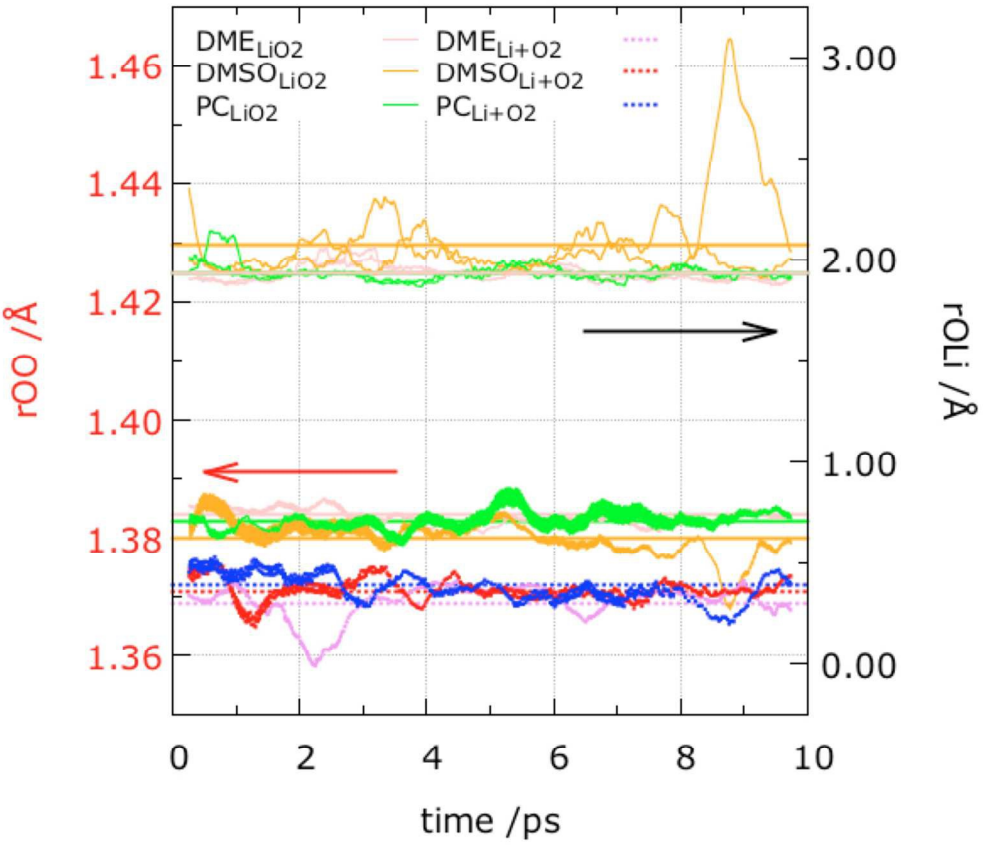

Figure 5 Running averages (0.5 ps, solid) and total averages (dashed) of rOO (bottom) and rOLi (top) bond length trajectories in DME, DMSO, and PC from DFT-MD simulations, T=353K, t=10 ps.
209x183mm (144 x 144 DPI)

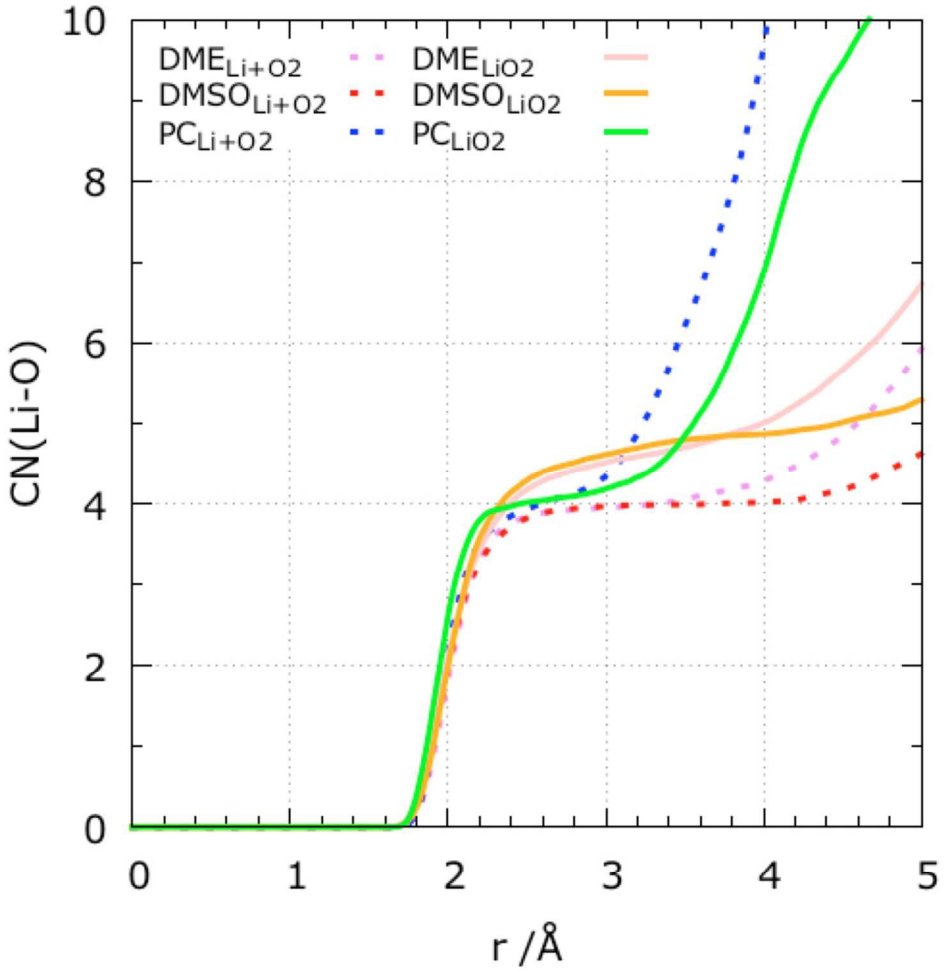

Figure 6 Coordination number of Li^+ in CIP (solid) and SSIP (dashed) electrolytes from DFT-MD simulations, T=353K, t=10 ps. Only the oxygen atoms are plotted for clarity. DME (pink, violet), DMSO (orange, red), and PC (green, blue).
183x183mm (144 x 144 DPI)

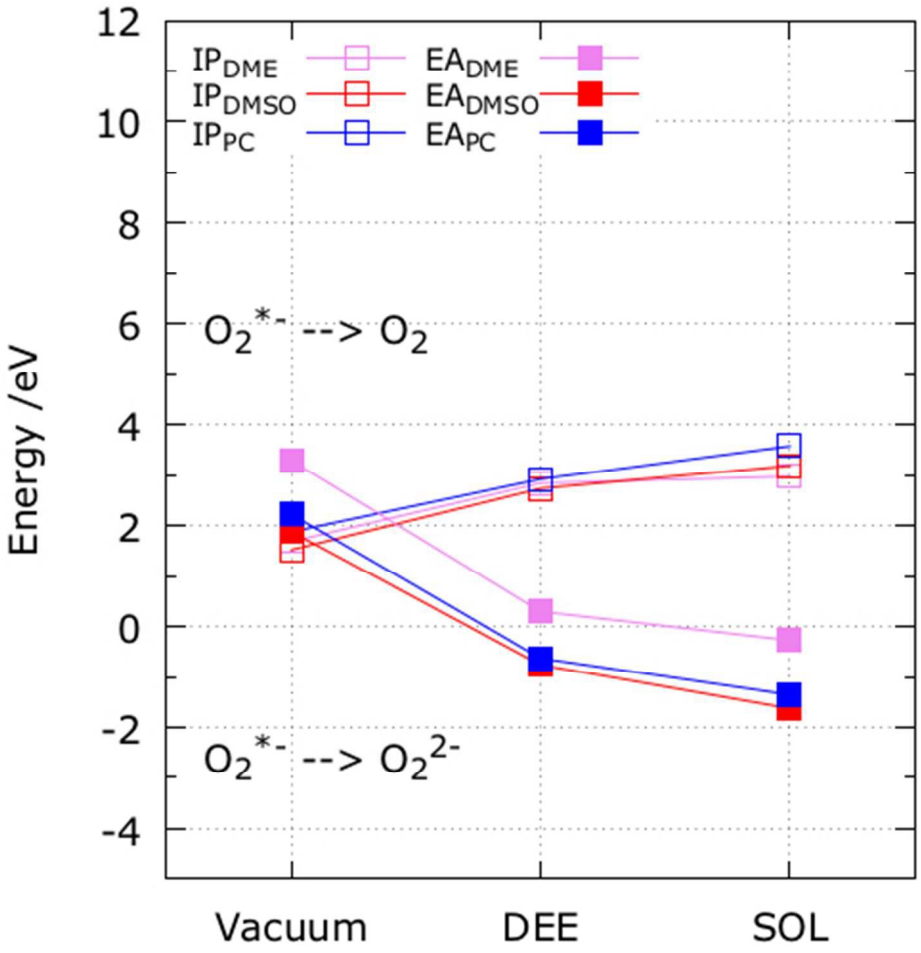

Figure 7 Ionization potentials (IP) and Electron affinities (EA) of clusters of O_2^{*-} explicitly solvated by six molecules of DME, DMSO, or PC, as function of an additional PCM continuum (vacuum, DEE, or SOL=DME, DMSO, or PC). All data are based on optimized energies of the oxidation/reduction products. B3LYP/6-31G(d).
184x184mm (72 x 72 DPI)

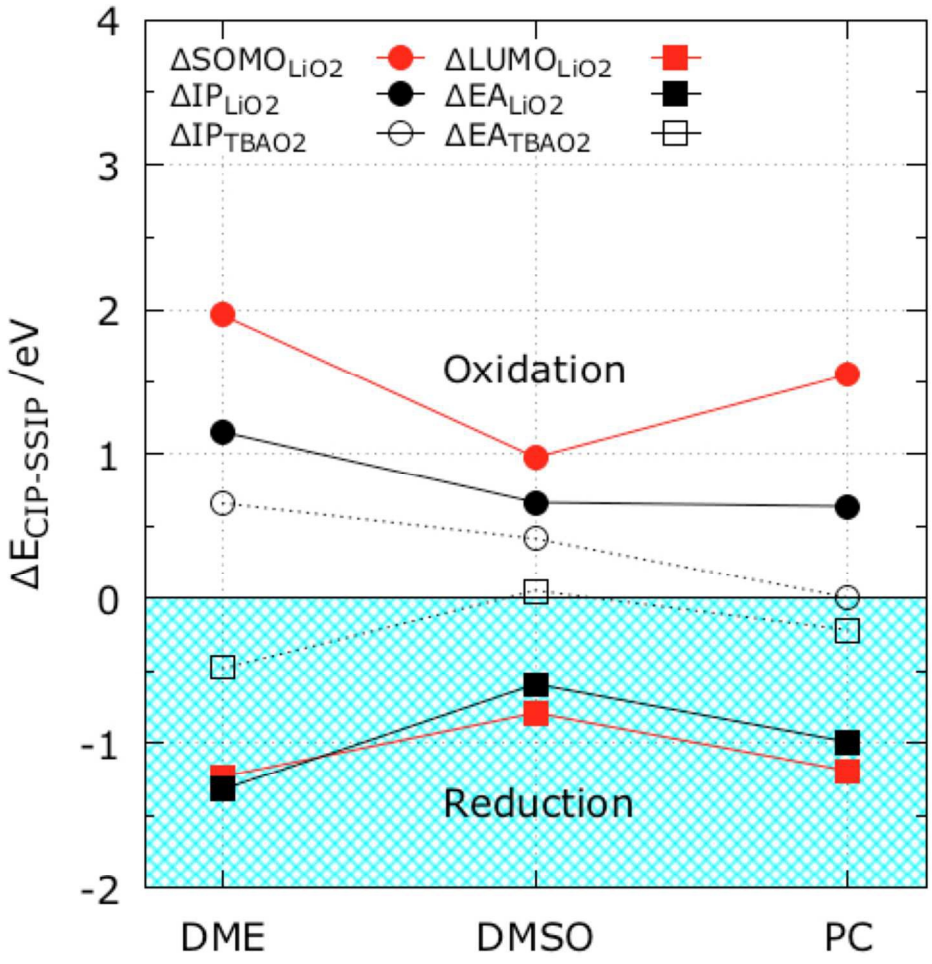

Figure 8 Changes in Ionization potentials (ΔIP, circles) and Electron affinities (ΔEA, squares) at CIP formation: LiO_2^{*}/O_2^{*-} (solid, black) and $[TBA]^{+}[O_2]^{*-}/O_2^{*-}$ (open, black) as a function of solvent (explicit + implicit). B3LYP/6-31G(d). DFT-MD ΔSOMO (red circles) and ΔLUMO (red squares) are included for reference.
182x182mm (144 x 144 DPI)